JOURNAL OF CATALYSIS 154, 151–162 (1995)

# Transient Kinetics from the TAP Reactor System: Application to the Oxidation of Propylene to Acrolein

Glenn Creten, David S. Lafyatis, and Gilbert F. Froment

*Laboratorium voor Petrochemische Techniek, Rijksuniversiteit Gent, Ghent, Belgium*

Received August 29, 1994; revised December 6, 1994

**Transient kinetic data have been extracted by use of the Temporal Analysis of Products (TAP) reactor system. In the TAP reactor high resolution transient pulse experiments are performed under vacuum conditions. A rigorous model is developed and applied to the determination of Knudsen diffusivities from experiments with inert pulses. The model was applied to the catalytic oxidation of propylene over an industrial multicomponent bismuth molybdate catalyst. By fitting simulated curves to the experimentally observed response curves, kinetic parameters for the different elementary steps of the reaction were determined. It was shown that the adsorption of propylene is practically irreversible at reaction temperature and that $CO_2$ and acrylic acid are formed in consecutive reactions from propylene via acrolein. From the values for the kinetic parameters it is proven that under industrial conditions the adsorption of propylene is rate determining. The surface coverage under typical conditions is shown to be quite low. The kinetic model is successfully used for the simulation of a steady state reactor operating under industrial conditions.** © 1995 Academic Press, Inc.

## INTRODUCTION

Transient methods in catalytic research are often used to gain more insight into the reaction mechanism and kinetics of complex reactions. Frequently used methods include temperature-programmed desorption (TPD) and pulse or step response techniques under reaction conditions. The resolution of TPD and temperature programmed surface reaction (TPSR) experiments is related to the peak width, which is a function of the heating rate and limited by the detection sensitivity: the slower the heating rate, the lower the peak intensity. In these techniques the operating temperature often differs from the industrially used temperature range. The resolution of pulse and step response experiments is limited by the pulse width or step rise time and by the detector time resolution. Common pulse techniques have a time resolution on the order of 1 to 100 s. The TAP reactor was developed by Gleaves and Ebner (1) to perform pulse experiments with a time resolution on the order of 1 ms.

The high time resolution of the TAP reactor system is achieved by the use of high speed pulse values (pulse width of $\pm 500$ $\mu$s), a near-zero dead volume manifold, and a catalytic microreactor placed directly inside a high vacuum mass spectrometer detection chamber. The reactor is operated under low pressure and the transport occurs by Knudsen diffusion. The TAP response curves from a reacting pulse depend on several parameters describing (i) the Knudsen transport, (ii) the adsorption–desorption kinetics, and (iii) the reaction mechanism and kinetics.

The first theoretical work on the TAP system was reported by Gleaves *et al.* (2). The continuity equations accounted for Knudsen diffusion in the gas phase, first-order adsorption and desorption, and a first-order surface reaction. A numerical solution was developed for a Dirac input pulse. This model was applied to the adsorption–desorption kinetics of acrolein over $Bi_2MoO_6$. The acrolein response curve is retarded by the adsorption on the catalyst surface. The effect is increasing with lower temperature, since the desorption rate decreases. From the model a simple equation was developed for the average elution time of a component that undergoes adsorption and desorption

$$t_{avg} = \frac{L^2}{2D_e}\left(1 + \frac{k_a}{k_d}\right), \qquad [1]$$

where $k_a$ and $k_d$ represent adsorption and desorption rate constants ($s^{-1}$), $L$ is the catalyst bed length, and $D_e$ is the Knudsen diffusion coefficient. Using this equation and the first moments of the curves, an activation energy for desorption was estimated, assuming that the activation energy for adsorption is negligible. The model was not applied to reacting pulses.

A more detailed, numerical model was developed by Svoboda *et al.* (3). The continuity equation for a component undergoing single first-order gas phase reaction was written, and the boundary condition at the reactor inlet corresponded to a forcing function for the flux. This model



0021-9517/95 $6.00

was applied to fit inert pulses and reactant pulses for $Me_3Sb$ and $Me_4Sn$ pyrolysis. Attempts to fit product curves from the pyrolysis reaction were unsuccessful.

The production of acrolein from propylene is a major industrial process, with a yearly production of 130,000 tons of acrolein in 1985 (4). It uses a multicomponent catalyst, developed from the earlier bismuth molybdate catalysis introduced in 1957 by the Standard Oil of Ohio Co. (SOHIO). Selectivities for acrolein above 85% are achieved at conversions between 90 and 95%. Metals added in recent catalysts often include Fe and Co. Millet *et al.* (5) showed the importance of synergy between Bi molybdates and Fe–Co molybdates for the performance of these catalysts. The $Fe^{2+}/Fe^{3+}$ redox couple promotes the $e^-$ and O-transfer. It has been shown that the oxygen incorporated in the acrolein originates from the lattice (6–8). $CO_2$ is formed from lattice oxygen or from both lattice and gas phase oxygen (6, 7). The catalyst oxygen participation in the reaction extends to something like 100 monolayers (9). The reaction mechanism involves an intermediate allylic surface species, as shown by experiments with deuterated propylenes and allyl radical generating components such as allyl alcohol, azopropylene, and allyliodide (10–13). The H-abstraction leading to the allylic intermediate is believed to take place at the O centers coordinated to Bi or at Bi–O–Mo bridge oxygen centers (12–14). The second H-abstraction and O-insertion, with formation of acrolein, are believed to occur at Mo–O–Mo bridge oxygen centers (12, 14, 15). The formations of $CO_2$ and acrylic acid would be consecutive steps, initiating from an adsorbed acrolein precursor (11).

The kinetics of this reaction have not been thoroughly investigated. There is no consistency in the published activation energies (16, 17), possibly due to differences in catalyst and temperature ranges investigated. The first H-abstraction, forming the allylic intermediate, is believed to be rate determining at high temperatures and industrial $O_2$ partial pressures (10, 11). However, at low temperatures, low $O_2$ partial pressures, or high $H_2O$ vapor contents, the catalyst reoxidation is found to be the slowest step in the mechanism (16–18). The reoxidation kinetics of a $\gamma$-$Bi_2MoO_6$ catalyst have been investigated earlier already by TAP (19) and an activation energy for reoxidation of the catalyst was determined. The activity of the catalyst for propylene oxidation was tested by means of anaerobic propylene pulses. Pulse response curves for the main products acrolein, $CO_2$, and $H_2O$ were obtained.

In the present study, the TAP pulse reactor system was used to investigate the kinetics of each elementary step of the oxidation of propylene into acrolein.

## EXPERIMENTAL

A schematic diagram of the TAP reactor system is given in Fig. 1. The microreactor, pulse valves, and quadrupole mass spectrometer are placed in a high vacuum system. The high vacuum ($\approx 10^{-9}$ bar) is maintained by two oil diffusion pumps and a turbo-molecular pump. When the inlet pulses are small ($< 5 \times 10^{15}$ molecules), the transport in the reactor occurs exclusively by Knudsen diffusion. The mass spectrometer measures the intensity and, therefore, the flux of a specified component of the effluent (*m/e* value) as a function of time. A typical experiment comprises a series of pulses. The response curves are then averaged to improve the signal to noise ratio. A typical response curve for an inert component (argon) is shown in Fig. 2. When a reaction is studied, several components must be monitored. Since only one *m/e* value can be monitored at a time, response curves for each component are obtained from duplicate pulse experiments, monitoring the appropriate *m/e* values. A high pressure assembly can be placed against the reactor outlet to allow experiments under a pressure of up to 2 bar. In this case a small portion of the reactor effluent is directed

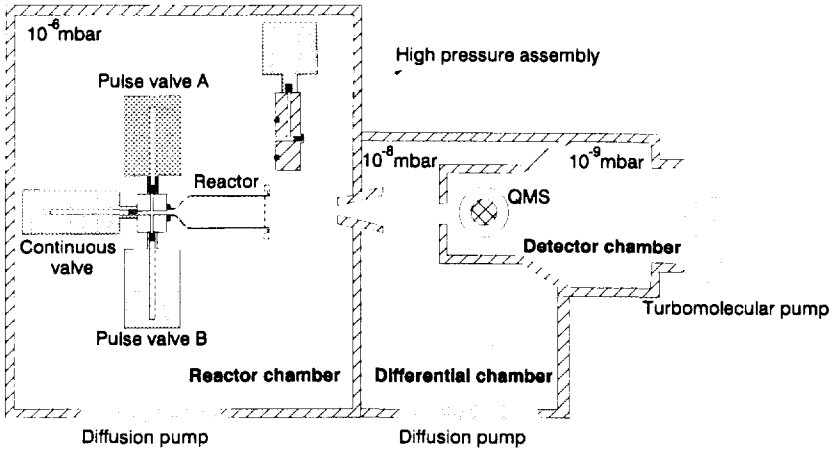


FIG. 1. Schematic diagram of the TAP reactor system.

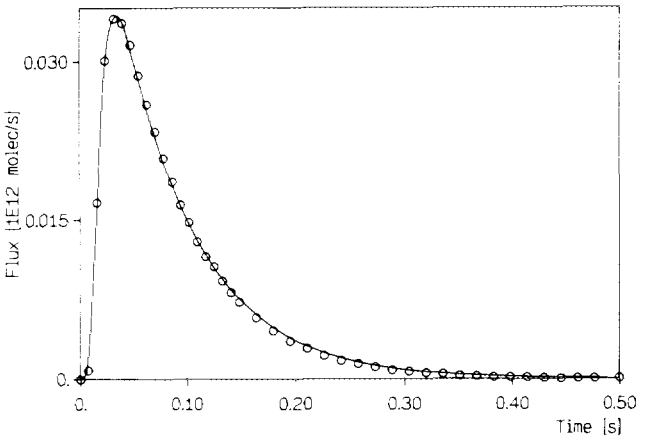


FIG. 2. Response curve of inert argon pulse over the catalyst bed at 451°C. Symbols are experimental data; line represents simulated response curve.

through a 0.001-in. pinhole leak and then immediately toward the mass spectrometer.

The TAP was used to investigate the oxidation of propylene to acrolein over an industrial multicomponent catalyst of the type $Co_{10}Mo_{12}Fe_1Bi_1O_y$, supplied by Rhône-Poulenc. The catalyst is prepared by reaction between an aquous solution of ammonium heptamolybdate $(NH_4)_6Mo_7O_{24}\cdot 4H_2O$ and a solution of Co, Bi, and Fe nitrates, followed by subsequent calcinations at 450 and 480°C for 6 h each. The catalyst is then pretreated in a conventional steady state reactor by a flow of propylene and air with a propylene to oxygen ratio of 1:2 for 200 h at 370°C. The TAP reactor has an inner diameter of 5.5 mm and a length of 40 mm. For the TAP pulse experiments 1.00 g of catalyst with a particle size 0.25–0.50 mm was used, corresponding to a catalyst bed length of 25 mm. The bed has a density of 1415 kg cat/$m_r^3$ and a void fraction of 0.38 $m_f^3/m_r^3$. The reactor was packed as shown in Fig. 3. The quartz particles at the reactor inlet and outlet are insulating, so that axial heat losses are minor. The SiC particles are highly conductive, thus reducing radial temperature profiles. In this way temperature gradients in the catalyst bed can be limited to approximately 2–5°C, depending on the operating temperature. The inert beds

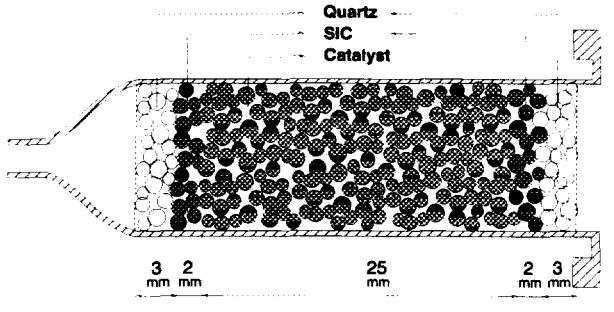


FIG. 3. Schematic representation of reactor packing.

also consisted of 0.25- to 0.50-mm particles. The TPD and TPSR experiments were performed on a short catalytic bed (0.08 g catalyst and 2-mm bed length) to avoid readsorption effects.

To calculate conversion and selectivities a calibration of the QMS was necessary for each component. For gases ($O_2$, $CO_2$, and propylene) a continuous flow was sent over an inert bed, and the signal of the QMS at the corresponding selected AMU was taken. A calibration factor (As/mol) was then calculated as the ratio between the QMS signal (A) and the molar flow (mol/s). For liquids (acrolein, acrylic acid, and allyl alcohol) a small amount (typically 10 $\mu$l) was introduced into the continuous-feed line through a septum. The selected AMU was then monitored until the entire sample had evaporated and eluted from the reactor. The QMS signal was then integrated, and the calibration factor (As/mol) was calculated from the ratio between the integrated signal (As) and the amount of liquid injected (mol). The $m/e$ values chosen as representative for each component, based on sensitivity and specificity, were 41 (propylene), 56 (acrolein), 44 ($CO_2$), 18 ($H_2O$), and 72 (acrylic acid).

## RESULTS

Continuous flow experiments under vacuum conditions with a 2:1 oxygen/propylene mixture were performed. The temperature was continuously varied at a rate of 1°C/min from 450 to 200°C. The total flow rate amounted to $3 \times 10^{-6}$ mol/s. Peaks in the mass spectrum related to propylene, acrolein, $CO_2$, $H_2O$, and acrylic acid could be determined. In Fig. 4 conversion and yields for the main products are given as a function of temperature. A similar continuous flow experiment was performed under 1 bar total pressure and a total flow rate of $9 \times 10^{-5}$ mol/s. The conversion and selectivities are given in Fig. 5. The results are quite comparable to those of the low pressure case. The lower conversion in the 1 bar experiment is caused by the shorter average residence time in the catalyst bed. The lower conversion also leads to lower selectivities for acrylic acid and $CO_2$, which will be shown to be formed in consecutive reactions from acrolein.

Pulse experiments with propylene at different temperatures were performed in the absence of oxygen. The responses of acrolein and $CO_2$ as well as that of unreacted propylene were detected by the QMS. Water was not detected satisfactorily in the pulse experiments because of the very broad response curve and the relatively high QMS background at $m/e$ = 18. The normalized responses for propylene, acrolein, and $CO_2$ at 412°C are shown in Fig. 6. Each curve consists of the averaged responses of 20 pulses, to improve the signal to noise ratio. Under these conditions it was observed that the catalyst properties remained constant for many pulse cycles, thus allowing

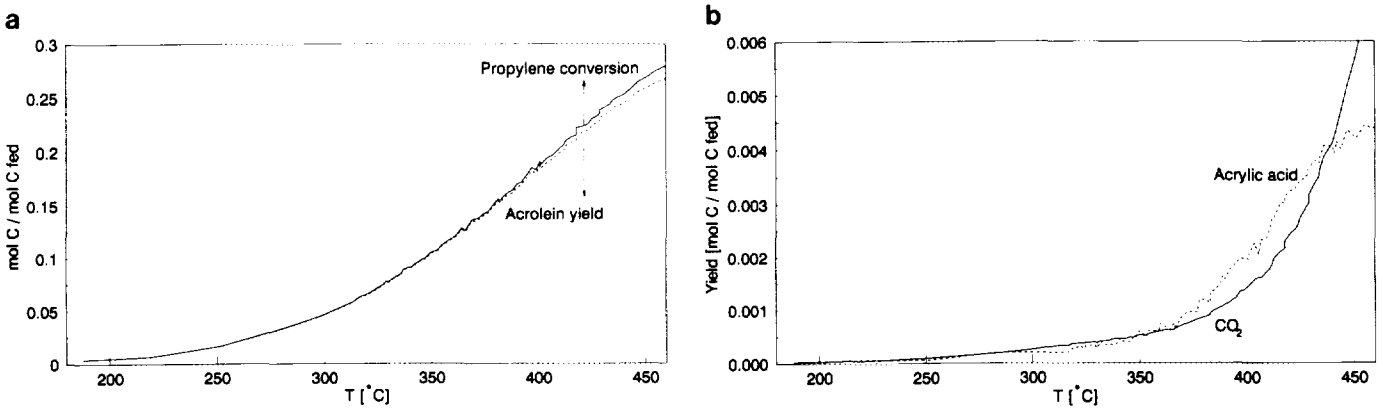


FIG. 4. Steady state propylene conversion and product selectivities under low pressure conditions as a function of temperature. (a) Propylene conversion and acrolein yield; (b) acrylic acid and $CO_2$ yields.

the same catalyst bed to be used for several experiments at different temperatures without reoxidation. To determine the role of desorption rate and readsorption in the acrolein response, acrolein was pulsed under the same conditions as the propylene pulses. $CO_2$ was the only product detected in this case. The normalized acrolein and $CO_2$ responses at 412°C are shown in Fig. 7.

Several temperature-programmed desorption and surface reaction (TPSR) experiments were performed to investigate the desorption characteristics of the relevant components. From the pretreated catalyst about $1.0 \times 10^{-4}$ mol $CO_2$/g catalyst desorbed in two peaks at 380 and 490°C, with a temperature ramp of 5°C/min. This $CO_2$ originates from strongly bound carbonaceous surface species. The existence of such species on bismuth molybdate catalysts has been previously observed (20, 21). No products other than $CO_2$ were detected.

The catalyst was treated with a propylene/$O_2$ mixture in a 1:2 ratio at 130°C for 20 min. After a 5-min equlibration period under vacuum, a temperature ramp of 10°C/min was started. The products detected were acrolein at 211°C, $H_2O$ at 225°C, and $CO_2$ as a broad peak at 360°C (Fig. 8).

Upon dosing the catalyst with an acrolein/$O_2$ mixture at 100°C, no desorption peak of acrolein was observed.

Acrylic acid was adsorbed at 100°C on a pretreated catalyst. Product peaks detected during a temperature ramp of 10°C/min were acrylic acid at 330°C and $CO_2$ at 360°C.

After treatment of the catalyst with allyl alcohol at 100°C, the TPSR spectrum showed peaks of allyl alcohol, acrolein, $CO_2$, and a minor amount of propylene. The catalyst was quickly saturated, since treatments for different time periods led to the same amount of desorbed products. Assuming that allyl alcohol is adsorbing on the same sites as propylene, this result can be used to calculate the total number of sites on the catalyst surface. This is justified by the fact that both components are adsorbed as the same allylic intermediate. A value of 0.07 mol/kg catalyst was found.

The response of acrylic acid was very broad and too small to be detected in pulse experiments. However, the slow formation of acrylic acid was revealed by transient step responses over a 1.00-g catalyst bed. A step in the propylene/$O_2$ flow was imposed by pulsing both pulse valves with, respectively, propylene and oxygen at a rate

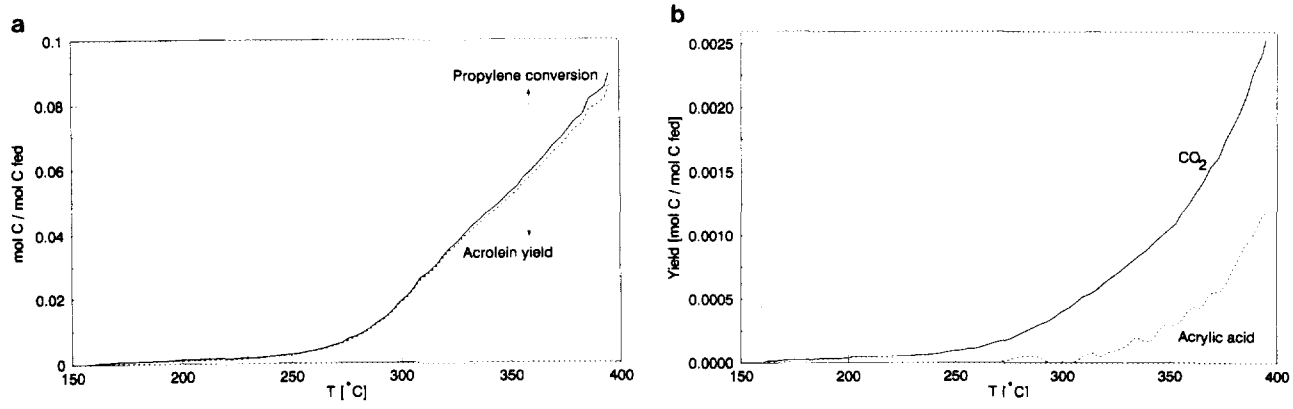


FIG. 5. Steady state propylene conversion and product selectivities under 1 bar total pressure as a function of temperature. (a) Propylene conversion and acrolein yield; (b) acrylic acid and $CO_2$ yields.

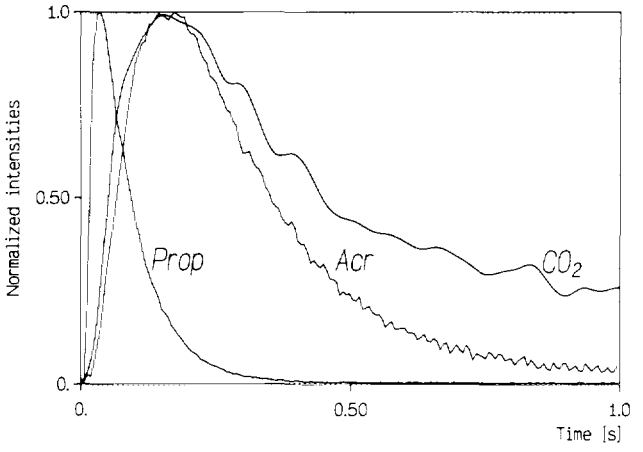


FIG. 6. Pulse responses of propylene, acrolein, and $CO_2$ on a propylene pulse at 412°C.

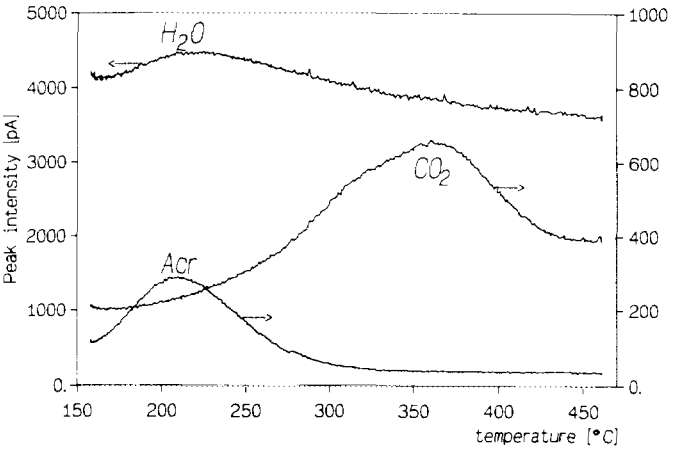


FIG. 8. TPSR of a Co–Fe–Bi–molybdate catalyst loaded with a propylene/$O_2$ mixture, temperature ramp of 10°C/min.

of 40 pulses per s. As can be seen from the propylene response in Fig. 9a, this leads to a step with a rise time of less than 200 ms. The acrolein and acrylic acid step responses at 424°C are shown in Figs. 9a and 9b. The rise time of the acrylic acid response is about two orders of magnitude higher than that of acrolein. This implies that the formation of acrylic acid is significantly slower than the formation of acrolein.

Additional step response experiments with propylene/oxygen and acrolein/oxygen steps have been performed over a short catalyst bed (3.5 mm) containing 0.14 g of catalyst. In this case the response signals rose to steady state values with a propylene conversion of 4% at 424°C. From the propylene step, the acrylic acid signal stayed below the detection limit. At 424°C, the acrolein feed was partially converted to acrylic acid and $CO_2$. The steady state conversion amounted to 1.2% with a selectivity of 52% for acrylic acid. This indicates that acrylic acid is formed in a consecutive reaction from propylene via acrolein.

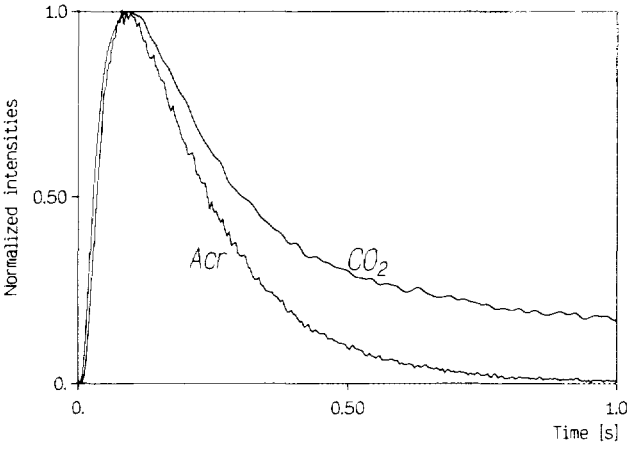


FIG. 7. Pulse responses of acrolein and $CO_2$ on an acrolein pulse at 412°C.

## MODELING

The model presented in this paper describes the simulation of an arbitrary network of elementary surface reaction steps for a reactor loaded as previously specified with an inert section, a catalyst, and again an inert section. First, it is assumed that the flow regime can be described by Knudsen diffusion. The Knudsen diffusion regime exists under conditions where the ratio between the mean molecular free path and average channel diameter exceeds a value of 0.63 (22). In a typical TAP pulse experiment this condition is satisfied for pressures below 100 Pa, and pulse sizes of up to $5 \times 10^{15}$ molecules (23). A rigid check on the validity of this assumption is the independence of pulse response shapes on the pulse size, for only in the Knudsen flow regime is the transport rate independent of pressure. The inlet pulse is assumed to be of negligible width, so that it can be described by a Dirac function. This presumes that the inlet pulse width is at least two orders of magnitude smaller than the response time. Indeed, in the present experiments the response curves had a width of at least 50 ms, while the inlet pulse had a width of 200 to 500 $\mu$s. A third assumption is that the degree of surface coverage is negligible. This can easily be accepted since a typical pulse size is $10^{15}$ molecules, while the amount of catalyst in the reactor is on the order of 1 g, usually corresponding to more than $10^{18}$ sites. The only restriction consists in the type of reaction steps considered. To avoid time-consuming numerical integration, the integration is performed by means of complex transforms, whose application is limited to first-order elementary reaction steps. This is only a minor restriction to the application of the model, since elementary steps may usually be considered to be pseudo-first-order in the reacting species.

The one-dimensional continuity equations in the catalytic bed for a component $i$ in the gas phase and adsorbed

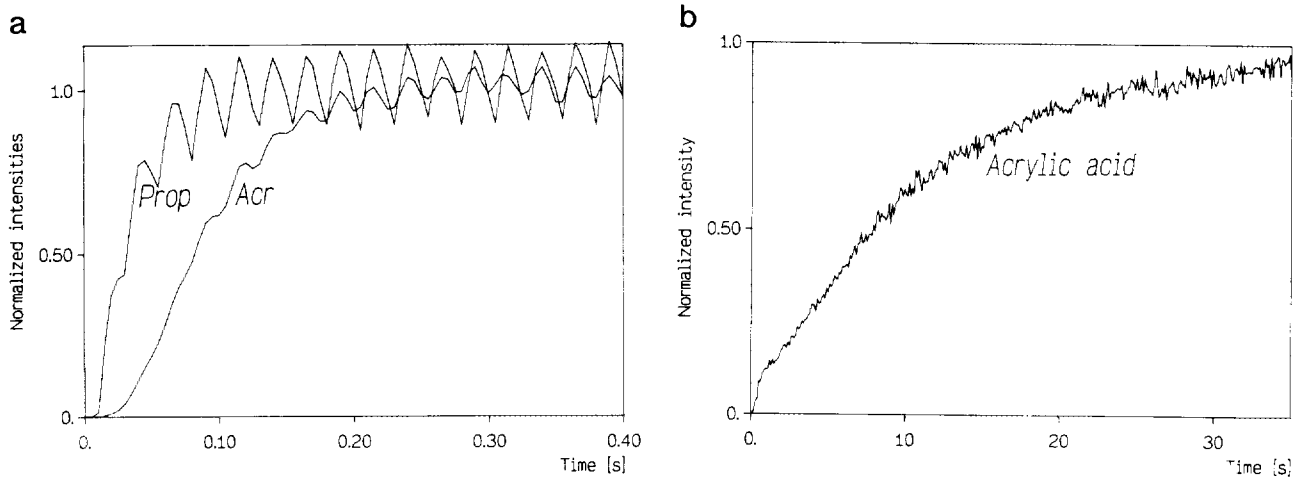


FIG. 9. Product step responses on a propylene step at 424°C (a) propylene and acrolein responses, (b) acrylic acid response.

on the surface are given by

$$\varepsilon \frac{\partial c_i}{\partial t} = D_{e_i} \frac{\partial^2 c_i}{\partial x^2} - \varepsilon k_{ads_i} c_i c_t + \rho_B k_{des_i} c_{ads_i}$$
$$\rho_B \frac{\partial c_{ads_i}}{\partial t} = \varepsilon k_{ads_i} c_i c_t - \rho_B k_{des_i} c_{ads_i} + \rho_B \sum_j \nu_{ij} k_{sr_j} c_{ads,q_j}. \quad [2]$$

The rate constants for adsorption $k_{ads}$ are expressed in terms of kg cat/kmol·s; the desorption and reaction rate constants $k_{des}$ and $k_{sr}$ are expressed in units of $s^{-1}$. The stoichiometric coefficient of component $i$ in reaction $j$, which is first-order in the surface species concentration $c_{ads,qj}$, is represented by $\nu_{ij}$ whereas $D_{e,i}$ ($m_f^3/m_r s$) denotes the Knudsen diffusion coefficient for component $i$. The one-dimensional gas phase continuity equation in the inert sections is derived from [2] by ignoring the terms for adsorption and reaction

$$\varepsilon \frac{\partial c_i}{\partial t} = D_{e_i} \frac{\partial^2 c_i}{\partial x^2}. \quad [3]$$

No continuity equation for adsorbed species is necessary in the inert sections.

The initial and boundary conditions for the reactor are

$$t = 0: \quad c_i = 0, \quad \forall i$$
$$c_{ads_i} = 0, \quad \forall i$$
$$x = 0: \quad -D_{e_i} \frac{\partial c_i}{\partial x} = \frac{\delta(t-\tau) N_p}{A_r}, \quad i = 1 \quad \text{(reactant)}$$
$$= 0, \quad i \neq 1 \quad \text{(products)}$$
$$x = L: \quad -D_{e_i} \frac{\partial c_i}{\partial x} = u_i^x \Omega_f c_i, \quad \forall i.$$

The boundary condition at the inlet ($x = 0$) states that the flux of component $i$ at the inlet corresponds to a Dirac function. The boundary condition also accounts for a dead time $\tau \approx 3$ ms, which has also been experimentally observed and may be attributed to delays in the pulse valve and the detection system, and to the transport time between reactor outlet and detector. The boundary condition at the exit of the reactor states that the flux leaving the reactor bed equals the flux that enters the vacuum system through the screen that holds the bed, with a free surface $\Omega_f$ of 0.34 $m_f^2/m_r^2$. The mean molecular velocity in one direction $u_i^x$ is calculated from the Maxwell velocity distribution:

$$u_i^x = \frac{u_i}{\sqrt{3}} = \sqrt{\frac{8RT}{3\pi M_i}}. \quad [5]$$

Additional boundary equations expressing continuity of concentrations and fluxes at the boundary planes between the inert sections and the catalyst bed are necessary. These are:

$$x = L_{boundary}: \quad c_i^{L_{boundary}^-} = c_i^{L_{boundary}^+}$$
$$D_{e_i}^{L_{boundary}^-} \frac{\partial c_i}{\partial x}\bigg|_{L_{boundary}^-} = D_{e_i}^{L_{boundary}^+} \frac{\partial c_i}{\partial x}\bigg|_{L_{boundary}^+}. \quad [6]$$

The set of partial differential equations [2] and [3] with boundary conditions [4] and [6] is solved by Laplace transformation with respect to time. The resulting set of ordinary differential equations in the Laplace domain is integrated analytically and the fluxes at the reactor outlet are calculated for different imaginary values of the Laplace variable $s$, thus giving discrete values of the Fourier transform. The flux profile in the time domain is then calculated by an inverse fast fourier transform algorithm (24).

To fit the model to the experimental observed response curves, parameters were estimated by means of the Levenberg–Marquardt algorithm. The 95% confidence intervals on these parameter values are estimated from calculated $t$-values by a linearization of the optimization function around the optimum.

The integration of the differential equations through Laplace transformation and the Levenberg–Marquardt optimization were implemented in a C-program on a HP-9000 workstation (23).

## DISCUSSION

The model for the TAP pulse reactor was first tested for inert pulses. A number of experiments were performed over an inert bed with components having masses between 28 ($N_2$) and 132 (Xe). The bed temperature was varied between 20 and 800°C. The Knudsen diffusivities for different components at different temperatures can be related to each other using the equation

$$D_e = D_e^0 \cdot \sqrt{\frac{T}{T^0} \cdot \frac{M^0}{M}} \qquad [7]$$

This relation holds as long as the flow regime is Knudsen diffusion, i.e., when the pulses are sufficiently small. The value $D_e^0$, related to a molecular mass $M^0$ and a temperature $T^0$, only depends on the size distribution and shape of the particles and the density of the packing. The validity of [7] was checked by fitting all of the inert pulses simultaneously, using a single diffusivity value of $2.69 \times 10^{-3}$ $m_f^3/m_r s$ for argon ($M$ = 40) at 40°C as a parameter. This value was converted by means of Eq. [7] to the appropriate mass and temperature for each curve. A number of experimental and simulated curves are shown in Figs. 10a and 10b.

The propylene pulse experiments were simulated using the TAP model described above, accounting for the reaction steps. First, the Knudsen diffusivity was calculated from argon pulses at 327 and 451°C over the reactor bed, i.e., 5 mm inert, 25 mm catalyst, and 5 mm inert particles (Fig. 2). Reference diffusivities were estimated for an argon pulse ($M$ = 40) at 350°C. Optimal values of $2.32 \times 10^{-3}$ and $2.63 \times 10^{-3}$ $m_f^3/m_r s$ were obtained for the diffusivities in the inert beds and the catalyst bed, respectively. The diffusivity for each of the reaction components was then estimated at the reaction temperature using Eq. [7].

The reaction scheme used for the modeling of the pulse experiments (Scheme 1) accounts for the adsorption of propylene (Prop) with formation, through H-abstraction, of the allylic intermediate (All Int), a second hydrogen abstraction and oxygen insertion, which are lumped into one surface reaction step, and desorption and readsorption of the acrolein precursor ($Acr_{ads}$).

In Scheme 1, the formation of carbon oxides ($CO_2$) and of surface carbon species ($C_{surf}$) may occur either as a parallel reaction from the allylic intermediate, or as a consecutive oxidation from the acrolein precursor. Acrylic acid (Acr Ac) has been shown previously to be formed in a consecutive reaction from the acrolein precursor only. As shown by Figs. 6 and 7, the $CO_2$ response curve has a long tail relative to the other response curves. In fact, the $CO_2$ response curve does not return to the baseline until after several seconds. This implies that the main part of the converted propylene that does not lead to acrolein remains adsorbed on the surface during many pulse cycles. From the mass balance it was seen that a significant amount of carbon stays irreversibly adsorbed on the catalyst surface. Therefore, the $CO_2$ curves from the propylene feed were not simulated with the other curves, but the formation rates of $CO_2$, surface carbon, and acrylic acid are lumped into one reaction step and

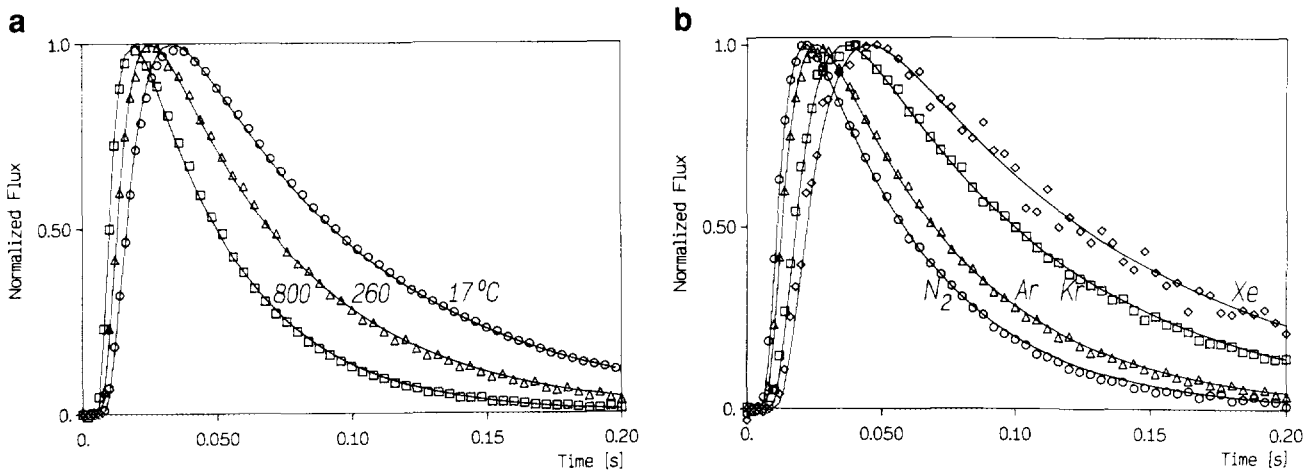


FIG. 10. Modeling of inert curves. Symbols are experimental data; lines represent simulated response curve. (a) Ar response curves at 800, 260, and 17°C; (b) $N_2$, Ar, Kr, and Xe response curves at 260°C.

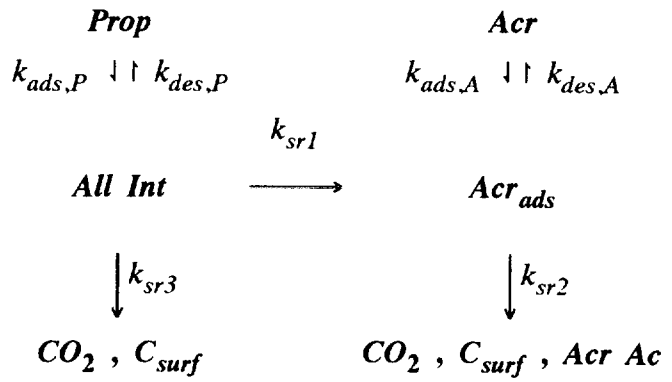


SCHEME 1. General reaction scheme for propylene oxidation.

TABLE 1

Optimal Parameter Values for Scheme 1

| Reaction step | Adsorption rate coefficient at 350°C ($s^{-1}$) | Activation enthalpy (kJ/mol) |
|---|---|---|
| $k_{ads,P}\,C_t$ | 1.04 ± 0.01 | 54.4 ± 0.3 |
| $k_{ads,A}\,C_t$ | 60 ± 25 | — |
| | Reaction rate coefficient at 350°C ($s^{-1}$) | Activation energy (kJ/mol) |
| $k_{sr1}$ | 4.61 ± 0.05 | 116 ± 1 |
| $k_{sr2}$ | 0.20 ± 0.02 | 115 ± 4 |
| $k_{sr3}$ | ($4 \times 10^{-6}$) | 0 |
| | Desorption rate coefficient $k_{des}$ at 350°C ($s^{-1}$) | Desorption enthalpy (kJ/mol) |
| $k_{des,P}$ | ($5 \times 10^{-8}$) | 0 |
| $k_{des,A}$ | 74 ± 3 | 77.8 ± 0.5 |

*Note.* Values between parentheses are not statistically significant.

estimated from the response curves of propylene and acrolein. Indeed, these curves contain all the information about the consumption of the allylic intermediate and adsorbed acrolein. To estimate the rate coefficients for the adsorption, desorption, and reaction steps from Scheme 1 both the responses on propylene and on acrolein pulses were used simultaneously. The responses on the propylene pulses do contain all necessary information for the parameter estimation, but by adding responses from acrolein pulses, the correlation between the parameters is diminished, so that they can be estimated with higher accuracy. Experimental data included propylene and acrolein responses on propylene pulses and acrolein responses on acrolein pulses at temperatures varying between 288 and 453°C. The results from this non-isothermal parameter estimation are shown in Table 1. The fit between experimental and simulated curves is shown in Figs. 11a and 11b.

The parameters in Table 1 reveal important characteristics of the reaction. First, the rate of the surface reaction $k_{sr1}$ is much higher than the rate of propylene desorption. This indicates that at reaction temperature, the adsorption of propylene leading to the allylic intermediate may be considered to be irreversible. Indeed, the parameters for propylene desorption were statistically nonsignificant. Table 1 also indicates that the rate of surface carbon formation from adsorbed acrolein is much larger than that from the allylic intermediate. The rate coefficient $k_{sr3}$ was not statistically significant, i.e., not different from zero. This result is consistent with Table 2, which shows that under identical reaction conditions the total amount of $CO_2$ formed from acrolein pulses was much larger than that from propylene pulses. The ratio of integrated responses of $CO_2$ and acrolein is nearly the same for both propylene and acrolein pulses, implying a consecutive pathway to $CO_2$ from propylene via acrolein.

As shown in Table 1, the desorption of acrolein occurs much more rapidly than the surface reaction ($k_{sr1}$), meaning that the latter is the slowest step *on the surface*. This conclusion was further checked by quantitative analysis

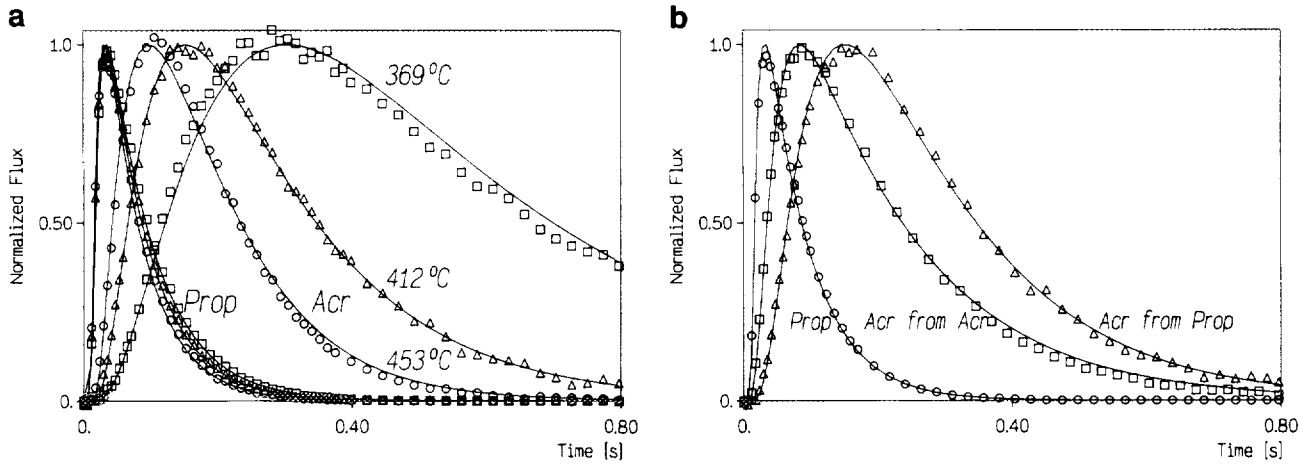


FIG. 11. Modeling of product responses from propylene and acrolein curves. (a) Propylene and acrolein responses from propylene pulses at 369, 412, and 453°C; (b) propylene and acrolein responses on propylene pulse and acrolein pulse at 412°C.

TABLE 2

**Integrated Product Responses of Propylene and Acrolein Pulses at 412°C**

| Input pulse | Composition of integrated responses | | | |
|---|---|---|---|---|
| | Propylene | Acrolein | $CO_2$ | $CO_2$/Acr |
| Propylene | 86.3% | 13.3% | 0.4% | 0.030 |
| Acrolein | — | 97.5% | 2.5% | 0.026 |

*Note.* Compositions are based on moles of carbon.

of the propylene TPSR experiment. The kinetic data of Table 1 were used to calculate a theoretical peak time for the acrolein response in the TPSR experiment with a propylene-loaded catalyst. The peak temperature $T_p$ is calculated from the Redhead equation for first-order desorption (25):

$$\frac{E_r}{RT_p^2} = \frac{A_0}{\beta} e^{-E_r/RT_p}. \qquad [8]$$

From the acrolein desorption parameters, shown in Table 1, a peak temperature of 188°C is obtained. With the preexponential factor and the activation energy for the surface reaction step $sr_1$, a peak temperature of 216°C is calculated. This is in excellent agreement with the observed peak at 211°C, thus showing that the appearance of acrolein in the propylene TPSR experiment is controlled by the rate of formation of adsorbed acrolein through reaction step $sr_1$.

*Application of the Low Pressure Pulsed Experiments to Steady State Operation at High Pressure*

The ultimate purpose of the kinetic study is the simulation of an industrial reactor. In the present paper the kinetic data derived from transient experiments under low pressure ($<10^{-3}$ bar) are shown to be applicable for the simulation of a reactor under completely different conditions. This is shown by a simulation of a steady state reactor under 1.6 bar total pressure.

It is useful to clearly define the relationship between the rate coefficients for adsorption, reaction, and desorption measured in the TAP system, and quantities in a steady state reactor. The surface reaction rate coefficients $k_{sr}$ and the desorption rate coefficients $k_{des}$ represent the frequency for each of these elementary steps occurring on the surface. The number of reaction steps occurring per unit of time and per site, often called the turnover frequency of the reaction, is given by

$$\frac{r_{sr}}{c_t} = k_{sr} \cdot \frac{c_{ads,i}}{c_t}, \qquad [9]$$

where $c_{ads,i}/c_t$ expresses the fractional surface coverage of the reacting species. Thus $k_{sr}$ and $k_{des}$ can be interpreted as maximum reaction or desorption rates, i.e., the rate when all catalyst sites are available for this specific elementary step.

To determine the rate-determining step under steady state conditions, the intrinsic rates for adsorption, surface reaction, and desorption have to be compared in magnitude. From the values of the kinetic parameters for $k_{des,A}$ and $k_{sr1}$ it can be concluded that the surface reaction is intrinsically much slower than the desorption of acrolein. The rate coefficient of adsorption $k_{ads,P}$ must be rescaled according to Eq. (2) before it can be compared to $k_{sr1}$. Under steady state conditions, the rates of adsorption and surface reaction must be equal:

$$\varepsilon \cdot k_{ads,P} \cdot c_l \cdot c_P = {}_B \cdot k_{sr_1} \cdot c_{All\ Int}. \qquad [10]$$

Thus, the steady state reaction rate is given by:

$$r_{SS} = k_{sr_1} \cdot c_{All\ Int} = \frac{\varepsilon \cdot (k_{ads,P} c_t) \cdot c_l \cdot c_P}{\rho_B \cdot c_t}. \qquad [11]$$

In the same way as the maximum reaction rate for the surface reaction is obtained at $c_{All\ Int} = c_t$, an equivalent maximum adsorption rate may be defined when the availability of adsorption sites is at its maximum, i.e., $c_l = c_t$. Thus, $k_{sr1}$ has to be compared in magnitude to the value of

$$\frac{r_{SS}}{c_l} = \frac{\varepsilon \cdot (k_{ads,P} c_t) \cdot c_P}{\rho_B \cdot c_t}. \qquad [12]$$

This value is now seen to scale directly with $k_{ads} c_t$, a quantity which is determined from the TAP experiments, shown in Table 1. A measure of the site density $c_t$ is still required. This was estimated from the allyl alcohol TPSR experiment previously described, with a result of 0.07 mol/kg cat. $r_{SS}/c_l$ is also dependent on reactor pressure, so it must be defined at a given set of feed conditions. Typical industrial conditions are 370°C and 0.1 bar propylene partial pressure. This gives a value for $r_{SS}/c_l$ of 0.0075 $s^{-1}$. This value is much lower than the rate coefficients for reaction and desorption, showing that the adsorption of propylene must be the rate-determining step under industrial conditions. This is in agreement with previous results (10, 11).

The rate coefficients shown in Table 1 may be used to predict the steady state coverage of the catalyst sites under given feed conditions as a function of propylene conversion. To do this, the simplified Scheme 2 is used, which ignores the reaction steps that where shown to be nonsignificant. The coverage of the surface by the side-products is ignored in the following derivation. This ap-

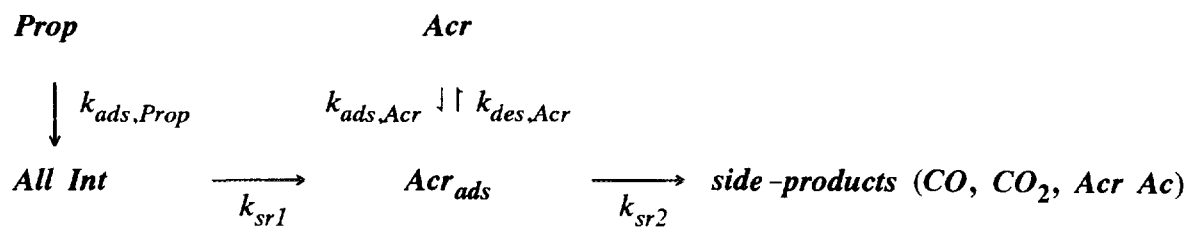


SCHEME 2. Simplified reaction scheme for propylene oxidation.

proximation is acceptable, given the high steady state acrolein selectivity achieved with this catalyst (>95%). The site-balance

$$c_{\text{All Int}} + c_{\text{Acr}_{ads}} + c_l = c_t \qquad [13]$$

is combined with the requirement that at steady state the forward rate of the various steps must be equal

$$r_{SS} = \frac{\varepsilon(k_{ads,P}c_t)^c{}_P c_l}{\rho_B{}^c{}_t} = k_{sr_1}c_{\text{All Int}} = (k_{des,A} + k_{sr_2})c_{\text{Acr}_{ads}} - \frac{\varepsilon(k_{ads,A}c_t)c_A c_l}{\rho_B c_t}. \qquad [14]$$

The solution of this set of equations allows the surface coverages of the allylic intermediate and of adsorbed acrolein to be calculated

$$\theta_{\text{All Int}} = \frac{c_{\text{All Int}}}{c_t} = \left(\frac{\varepsilon}{\rho_B c_t}\frac{(k_{ads,P}c_t)}{k_{sr_1}}c_P\right)\Big/\text{DEN} \qquad [15]$$

$$\theta_{\text{Acr}_{ads}} = \frac{c_{\text{Acr}_{ads}}}{c_t} = \left(\frac{\varepsilon}{\rho_B c_t}\left[\frac{(k_{ads,P}c_t)}{k_{des,A} + k_{sr_2}}c_P + \frac{(k_{ads,A}c_t)}{k_{des,A} + k_{sr_2}}c_A\right]\right)\Big/\text{DEN}, \qquad [16]$$

where

$$\text{DEN} = 1 + \frac{\varepsilon}{\rho_B c_l}\left(\frac{(k_{ads,P}c_t)}{k_{sr_1}} + \frac{(k_{ads,P}c_t)}{k_{des,A} + k_{sr_2}}\right)c_P + \frac{\varepsilon}{\rho_B c_t}\frac{(k_{ads,A}c_t)}{k_{des,A} + k_{sr_2}}c_A. \qquad [17]$$

Because of the dependence of the surface coverages on the partial pressures of propylene and acrolein, they can be expressed as a function of propylene conversion. For typical industrial feed conditions of 0.1 bar of propylene and 370°C, the surface coverages as a function of propylene conversion are shown in Fig. 12. It can be seen that the total surface coverage (allylic intermediate + acrolein) remains below 0.3%, even at complete conversion to acrolein. Figure 13 shows the total surface coverage as a function of temperature and conversion. The total surface coverage exceeds 5% only at temperatures below 270°C.

Finally, a steady state plug flow reactor was simulated based on the model presented in Scheme 2 and the kinetic data presented in Table 1. The rate equations are derived

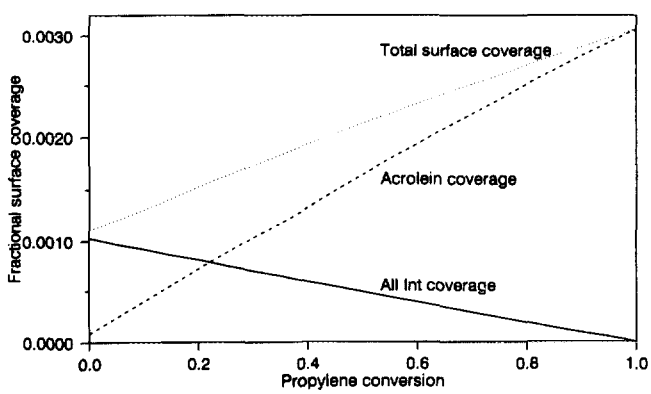


FIG. 12. Steady state surface coverage under industrial conditions (1 bar total pressure, 0.1 bar inlet pressure of propylene) at 370°C as a function of propylene conversion.

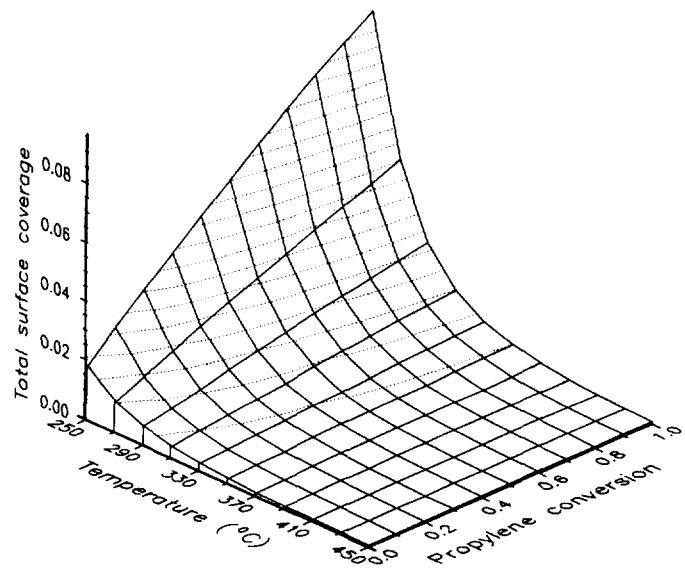


FIG. 13. Total surface coverage under industrial conditions (1 bar total pressure, 0.1 bar partial pressure of propylene) as a function of temperature and conversion.

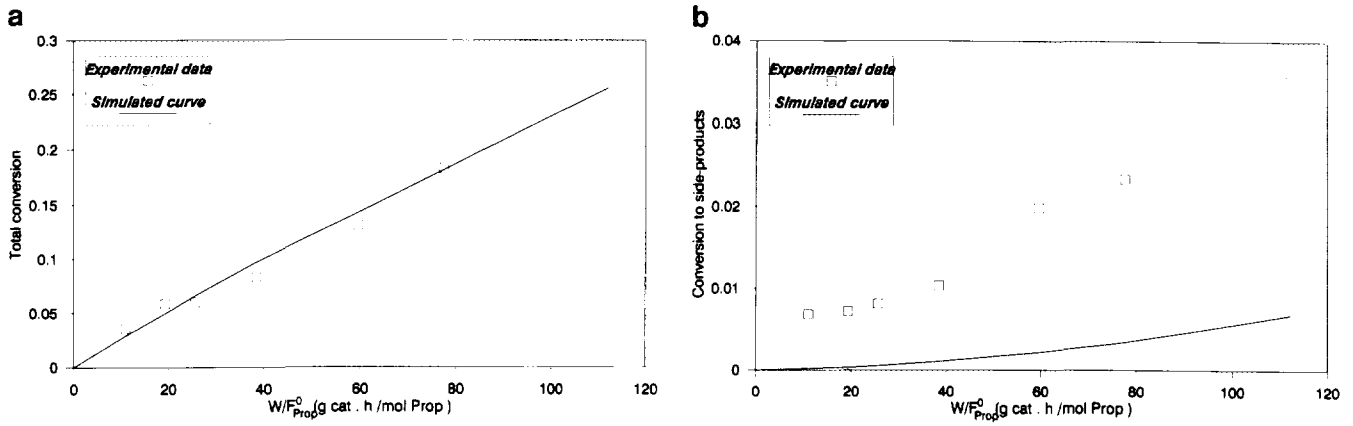


FIG. 14. Experimental and simulated conversions for bench scale steady state reactor at 1.6 bar total pressure and 350°C. (a) Total propylene conversion; (b) conversion to side-products.

immediately from Eqs. [14] through [17]. The bench scale steady state reactor consisted of a cylindrical tube of length 21.2 cm with a 1.8-cm diameter, containing 5.068 g of catalyst mixed with inert particles with a size of 0.75 mm. Reaction conditions are given in Table 3.

Figure 14 gives the experimental values and the calculated curves for the total conversion and the conversion to side-products as a function of the space time $W/F_P^0$. The calculated total conversions agree very well with the experimental data. The difference in selectivity must be attributed to the presence of gas phase oxygen in the steady state reactor. This indicates that part of the side-products, mainly $CO_2$, is formed in a reaction step with gas phase oxygen or physically adsorbed oxygen.

## CONCLUSIONS

A model has been developed to simulate the TAP pulse reactor. It was tested extensively for inert pulses, showing that under the chosen experimental conditions, the assumption of Knudsen diffusion is valid. The model was then applied to the oxidation of propylene over an industrial catalyst and the kinetic parameters were estimated. These parameters were extrapolated to atmospheric pressure conditions to show that the adsorption with H-abstraction is rate determining and that surface coverages under industrial conditions remain extremely low. The resulting kinetic data are shown to be applicable to the simulation of a reactor under industrial conditions.

TABLE 3

Steady State Reactor Experimental Data

| | |
|---|---|
| Reactor dimensions | |
| Tube length | 0.212 m |
| Internal diameter | 0.018 m |
| Catalyst particle size | 0.75 mm |
| Temperature | 350°C |
| Pressure | 1.6 bar |
| Catalyst loading | 5.068 g |
| Bed density | 93.9 kg/m³ |
| Feed composition | |
| $C_3H_6$ | 6.57 mol% |
| $O_2$ | 14.62 mol% |
| $N_2$ | 55.71 mol% |
| He | 23.10 mol% |

## APPENDIX: SYMBOLS

| | | |
|---|---|---|
| $A_0$ | ($s^{-1}$) | Preexponential factor |
| $A_r$ | ($m^2$) | Cross-sectional area of reactor |
| $c_i$ | (kmol/m³) | Gas phase concentration of component $i$ |
| $c_{ads,i}$ | (kmol/kg) | Surface concentration of adsorbed species $i$ on catalyst |
| $c_l$ | (kmol/kg) | Surface concentration of free sites on catalyst |
| $c_t$ | (kmol/kg) | Surface concentration of reactive sites on catalyst |
| $D_{e,i}$ | ($m^3/m_r$ s) | Effective diffusivity of component $i$ |
| $E_r$ | (J/kmol) | Activation energy |
| $k_{ads}$ | (kg/kmol s) | Adsorption rate coefficient |
| $k_{des}$ | ($s^{-1}$) | Desorption rate coefficient |
| $k_{sr}$ | ($s^{-1}$) | Reaction rate coefficient |
| $L$ | (m) | Reactor bed length |
| $M_i$ | (kg/kmol) | Molecular mass of component $i$ |
| $N_p$ | (kmol) | Pulse size |
| $r_{sr}$ | (kmol/kg s) | Reaction rate |
| $r_{SS}$ | (kmol/kg s) | Steady state reaction rate |
| $R$ | (8314 J/kmol K) | Ideal Gas Law Constant |
| $t_{avg}$ | (s) | Average elution time of a pulse response |

| | | |
|---|---|---|
| $T$ | (K) | Temperature |
| $T_p$ | (K) | TPD peak temperature |
| $u_i$ | (m/s) | Mean molecular velocity |
| $u_i^x$ | (m/s) | Mean molecular velocity in one dimension |
| $W$ | (kg) | Amount of catalyst |
| $x$ | (m) | Axial coordinate in reactor |
| $\beta$ | (°C/s) | Heating rate |
| $\delta(t)$ | ($s^{-1}$) | Dirac time function |
| $\varepsilon$ | ($m^3/m^3$) | Bed void fraction |
| $\rho_B$ | (kg cat/$m^3$) | Catalyst bed density |
| $\Omega_f$ | ($m^2/m^2$) | Free surface of screen at reactor outlet |

## ACKNOWLEDGMENTS

The present work was carried out under the IUAP-Center of Excellence Grant provided by the Belgian "Ministerie voor de Programmatie van het Wetenschappelijk Beleid." The authors thank Ir. V. Boschat for the bench scale reactor data and Mr. O. Dewaele for cooperation. The valuable discussions with Mr. P. Jaeger, Mr. H. Ponceblanc, and Mr. M. Garrait of Rhône-Poulenc are also acknowledged.

## REFERENCES

1. Gleaves, J. T., and Ebner, J. R., U. S. Patent 4,626,421, 1986, to Monsanto Co.
2. Gleaves, J. T., Ebner, J. R., and Kuechler, T. C., *Catal. Rev.-Sci. Eng.* **30**(1), 49 (1968).
3. Svoboda, G. D., Gleaves, J. T., and Mills, P. L., *Ind. Eng. Chem. Res.* **31,** 19 (1992).
4. Gerhartz, W. (Ed.), "Ullmann's Encyclopedia of Ind. Chem.," VCH, Germany (1985).
5. Millet, J. M. M., Ponceblanc, H., Coudurier, G., Herrmann, J. M., and Vedrine, J. C., *J. Catal.* **142,** 381 (1993).
6. Keulks, G. W., and Krenzke, *in* "Proceedings, 6th International Congress on Catalysis, London, 1976" (G. C. Bond, P. B. Wells, and F. C. Tompkins, Eds.), Vol. 2, p. 806. The Chemical Society, London, 1977.
7. Krenzke, L. D., and Keulks, G. W., *J. Catal.* **61,** 316 (1980).
8. Krenzke, L. D., and Keulks, G. W., *J. Catal.* **25,** 418 (1978).
9. One, T., Nakajo, T., and Hironaka, T., *J.Catal.* **36,** 240 (1975).
10. Adams, C. R., and Jennings, T. J., *J. Catal.* **2,** 63 (1963).
11. Boreskov, G. K., Erenburg, E. M., Andrushkevich, T. V., Zelenkova, T. V., Bibin, V. N., Meshcheryakov, V. D., Boronina, N. P., and Tyurin, Yu N., *Kinet. Katal.* **24**(3), 755, 198 (1982).
12. Grzybowska, B., Haber, J., and Janas, J., *J. Catal.* **49,** 150 (1977).
13. Burrington, J. D., Kartisek, C. T., and Grasselli, R. K., *J. Catal.* **63,** 235 (1980).
14. Glaeser, L. C., Brazdil, J. F., Hazle, M. A., Mehicic, M., and Grasselli, R. K., *J. Chem. Soc. Faraday Trans.* **81,** 2903 (1985).
15. Keulks, G. W., Krenzke, L. D., and Notermann, T. M., *Adv. Catal.* **19,** 232 (1970).
16. Monnier, J. R., and Keulks, G. W., *J. Catal.* **68,** 51 (1981).
17. Al'kaeva, E. M., Andrushkevich, T. V., and Meshcheryakov, V. D., *Kinet. Katal.* **32**(6), 1392 (1991).
18. Tichy, J., and Machek, J., *Catal. Lett.* **15,** 401 (1992).
19. Coulson, D. R., Mills, P. L., Kourtakis, K., Lerou, J. J. and Manzer, L. E., *Stud. Surf. Sci. Catal.* **72,** 305 (1992).
20. Grzybowska, B., Haber, J., Marczewski, W., and Ungier, L., *J. Catal.* **42,** 327 (1976).
21. Kobayashi, M., and Fytaya, R., *J. Catal.* **56,** 73 (1979).
22. Brown, *et al.*, *J. Appl. Phys.* **17,** 802 (1946).
23. Creten, G., Ph.D. Thesis, Rijksuniversiteit Gent., Ghent, 1994.
24. Press, W. H., Flannery, B. P., Teukolsky, S. A., and Vetterling, W. T., "Numerical Recipes." Cambridge Univ. Press, Cambridge, UK, 1986.
25. De Jong, A. M., and Niemantsverdriet, J. W., *Surf. Sci.* **233,** 355 (1990).